Research Article

X-RAY Spectrometry

Received: 19 January 2010 Accepted: 25 January 2010 Published online in Wiley Interscience: 28 March 2010

(www.interscience.com) DOI 10.1002/xrs.1246

A versatile Monte Carlo package for computation of efficiencies of Si(Li), SDD and Ge detectors

S. M. Taylor,† S. M. Andrushenko, J. M. O'Meara and J. L. Campbell*

Currently, most detector efficiency calculations for X-ray detectors assume that the source is a point source on the axis of symmetry of the detector, but this is not always accurate. We have devised a Monte Carlo program to simulate photon transport in Si(Li), SDD and planar Ge detectors that natively handles finite, tilted and off-axis sources. Although electron transport is not handled at this stage, photon transport is completely handled, including absorption from filters and multiple scattering in the detector crystal. The K escape peak is handled for both silicon and germanium detectors, and the L escape peak is also handled for germanium detectors. Our efficiency results compare very well with previous work when idealized systems are simulated, and the effect of a non-idealized system is presented. Escape peak intensity ratios are given for both silicon detectors (K peak only) and germanium detectors (K and L peaks), and the results for the K escape peaks agree well with previous work. Results are presented for a recent annular detector system, which is a good example of systems that are poorly handled under previous efficiency calculations.

Introduction

Using Monte Carlo simulations to determine detector efficiency is not a new idea: de Castro Faria and Levesque[1] and Wainio and Knoll[2] both did work on planar germanium detectors in the mid-1960s; Wainio and Knoll's work also covers silicon detectors. A simple efficiency model for planar Si(Li) and Ge X-ray detectors was introduced by Hansen *et al*.[3] and extended by Cohen.[4] It remains widely used, both in fundamental physics work and in the various modes of X-ray emission analysis of materials. Variants of it have been incorporated in computer packages that are used in X-ray fluorescence (XRF) and particle-induced X-ray emission (PIXE) analysis. Despite this widespread acceptance, the model contains several approximations. Remedies for some of these were proposed by O'Meara and Campbell[5] but other issues remain. In the present work, we have developed a Monte Carlo code that provides a more accurate prediction of efficiency as a function of X-ray energy; it is suitable for incorporation in XRF and PIXE packages.

Previous Work

The model of Hansen *et al*.[3] and Cohen[4] assumes a point source on the axis of the detector. It computes (1) X-ray transmission factors t_i, on that axis, through the various absorbers (possible air, window, contact, possible nitrogen filling, possible surface ice layer, possible silicon dead layer) that precede the actual detecting crystal and (2) X-ray absorption within the crystal itself. The solid angle Ω (in steradians), subtended by the photon source at the detector's front face, is included in the efficiency expression, and so it is the absolute efficiency $\varepsilon(E)$ that is calculated. The absorption factor is usually calculated using the photoelectron cross section in silicon. Thus, the efficiency can be calculated by

$$\varepsilon(E) = \frac{\Omega}{4\pi}(t_{\text{air}}t_{\text{w}}t_{\text{c}}t_{\text{i}}t_{\text{N}}t_{\text{DL}})[1 - e^{(-\mu_{\text{pe}}D)}]F_{\Omega}F_{\text{ESC}}F_{\text{CC}} \qquad (1)$$

F_{Ω} is a geometry-dependent factor that imparts an energy dependence to the solid angle in the case where the detector is not collimated; this expression may also include an approximate correction factor for a finite source. The absorption factor in square brackets represents the fraction of the remaining X-rays that interact by a single photoelectric absorption in the crystal, whose thickness (generally not known *a priori*) is D; μ_{pe} is the photoelectric linear attenuation coefficient of silicon. F_{ESC} represents the loss of intensity into the silicon K X-ray escape peak and has been accurately parameterized elsewhere.[6] The factor F_{CC} provides an entirely empirical means of representing the combined effects of photoelectron and Auger electron escape and charge carrier collection efficiency near the front contact.

There are several approximations implicit in Eqn (1). The F_{Ω} factor is approximate; it renormalizes the solid angle, with the source–crystal distance augmented by the mean interaction depth of the X-rays, conferring an energy dependence as noted above; the finite source size correction incorporated here is approximate. The angular spread of the X-rays is neglected as far as the transmission and absorption factors are concerned. The transmission factors for low-energy X-rays which proceed furthest off the axis of symmetry will therefore be underestimated.

* *Correspondence to: J. L. Campbell, Guelph-Waterloo Physics Institute, University of Guelph, Guelph, Ontario, Canada N1G 2W1. E-mail: jlc@physics.uoguelph.ca*

† *Present address: Department of Atmospheric and Oceanic Sciences, McGill University, Montreal, Quebec, Canada H3A 2T5.*

Guelph-Waterloo Physics Institute, University of Guelph, Guelph, Ontario, Canada N1G 2W1

The absorption term

$$f_{pe} = \left[1 - e^{-\mu_{pe}D}\right] \quad (2)$$

used in Eqn (1) is an approximation, because it ignores attenuation of the photon by coherent or Compton scattering. The exact expression for the intrinsic efficiency of the crystal, that is, the fraction of incident photons that interact by a single photoelectric absorption, is

$$f_{pe} = \frac{\mu_{pe}}{\mu_{tot}}\left[1 - e^{-\mu_{tot}D}\right] \quad (3)$$

When the photon energy is low, the simpler expression [Eqn (2)] closely approximates the correct expression [Eqn (3)]. However, with increasing energy, increasing error is incurred; for 20 keV photons and a 5-mm thick Si(Li) detector, the approximate term overestimates the exact term by 8–9%. Moreover, the model does not consider the possibility of a series of Rayleigh or Compton scatter interactions in the silicon being followed by a photoelectric event nor is such a scenario allowed for in the corrected expression of Eqn (3). Thus, for Si(Li) detectors, the efficiency is underestimated at X-ray energies above approximately 20 keV. Two of the present authors[5] used Monte Carlo simulations to generate tables of correction factors for this effect, but these have the inconvenience of requiring interpolation for the particular geometry at hand.

The analytical model does not deal with off-axis sources, and though it has an approximate correction for sources of finite area, it does not deal with such sources when their planes are not normal to the detector's cylindrical axis. These omissions are of some importance since the advent of annular arrays of silicon drift detectors. Additionally, the escape of silicon K X-rays is dealt with, but not the escape of silicon K Auger electrons or photoelectrons. It is left to the user to incorporate any knowledge of 'hot' (i.e. photo- and Auger) electron escape and charge carrier losses near the front contact via the empirically determined F_{CC} factor. Scholze and Procop[7] have recently described an approach in which they model the hot electron escape effects and then determine the charge carrier losses by fitting measured response functions as a function of X-ray energy. Finally, no attention is paid to the possibility of an electronic efficiency factor[8] caused by the event rejection circuitry or software.

Present Objective

In the context of the PIXE software package GUPIX[9] and similar packages for spectrum processing, it occurred to us to provide an alternative to the simple analytical model. This takes the form of a stand-alone 'black box' code which the user executes for a given experimental arrangement, and which provides a file of absolute efficiencies as a function of energy; this file can be stored for future use by the main spectrum processing code, which interpolates in it at the energies pertinent to the analytical application. The user first defines the detector parameters and the geometry, and inputs a list of desired X-ray energies. Each of these energy values is dealt with successively in the 'box' by a Monte Carlo computation for a large number of X-rays of that energy. This approach eliminates all the approximations inherent in the simple model described above, with two specific exceptions. Electronic efficiency cannot be addressed because it is a function of the individual electronic system, and issues of hot electron transport are not addressed at this stage of the work. In the next two sections, we describe the computational methodology and the database.

Program Functionality

This program was built to eliminate the various assumptions and geometric assumptions that characterized most previous work. The program itself is very straightforward: a photon is generated with the appropriate energy, it is propagated towards the detector through various filters (where it may be absorbed), and once it hits the detector it can interact any number of times until it deposits all the initial energy or it leaves the detector. A series of flags note both where the photon goes and if and where the photon is absorbed by one of the filters; this way, the user can clearly see the eventual fate of all the photons simulated. Once inside the crystal, the photon can scatter coherently or incoherently, undergo a photoelectric event, or it may pass through the detector without interacting. Note that there is no consideration of any scattering occurring in any of the absorbing layers; at the low X-ray energies where these filters (which typically have low atomic number) reduce the transmission significantly, the error induced by neglecting scattering effects is at the 0.1% level. The detectors considered here are useful only at energies well below the threshold of pair production, so these are the only three possible interactions. Typically, the silicon detectors are used below ~40 keV, and the germanium below ~100 keV. The database constructed for the program includes cross sections up to 100 keV for silicons crystals and up to 200 keV for germanium crystals.

If a photon induces a photoelectric event, the atom may undergo a K shell fluorescence event instead of the typical emission of an Auger electron. If this is the case, the fluorescent photon is also tracked until it deposits its energy or leaves the crystal; thus, the escape peak is rigorously modelled. If the fluorescent photon remains in the crystal, it can interact again, and a tally of the interactions (both number and type, for a complete characterization of the detector's response) is kept. Once the photon either deposits all its energy or leaves the crystal, the event is stopped, and the event is tabulated. The procedure of propagating and tracking a photon is described graphically in Figure 1.

Tabulating the event involves calculating the efficiency for the individual photon and incrementing the counts of photons with a similar fate. The program generates a specified number of photons at a given energy and outputs all the results in a series of detailed output files. The program loops over an input number of energies too, so the ultimate result is a vector of absolute detector efficiencies corresponding to a vector of source energies. The program outputs a series of files, all useful for different things; a sample of the most detailed file output is shown for a close to ideal geometry and a single energy in the Appendix. The complete description of the program's input/output structure is detailed in a program manual. This paper discusses the pertinent mechanics and calculations needed to eliminate the previous geometric restrictions, rather than the operational concerns.

A wide variety of detector systems can be analysed with this program, and a general setup is shown in Figure 2. The system can include a number of filters, namely, an ambient environment, a collimator on the outside of the detector window, a detector window, an environment within the detector casing, a collimator on the face of the detector, an ice layer on the detector, an electrode contact on the detector and a dead layer at the leading face of the detector crystal. The photon is assumed not to scatter in any of the filters it encounters before the detector crystal; it either passes through unchanged or it is absorbed. Not all of these components must be present: the user can specify the density (or

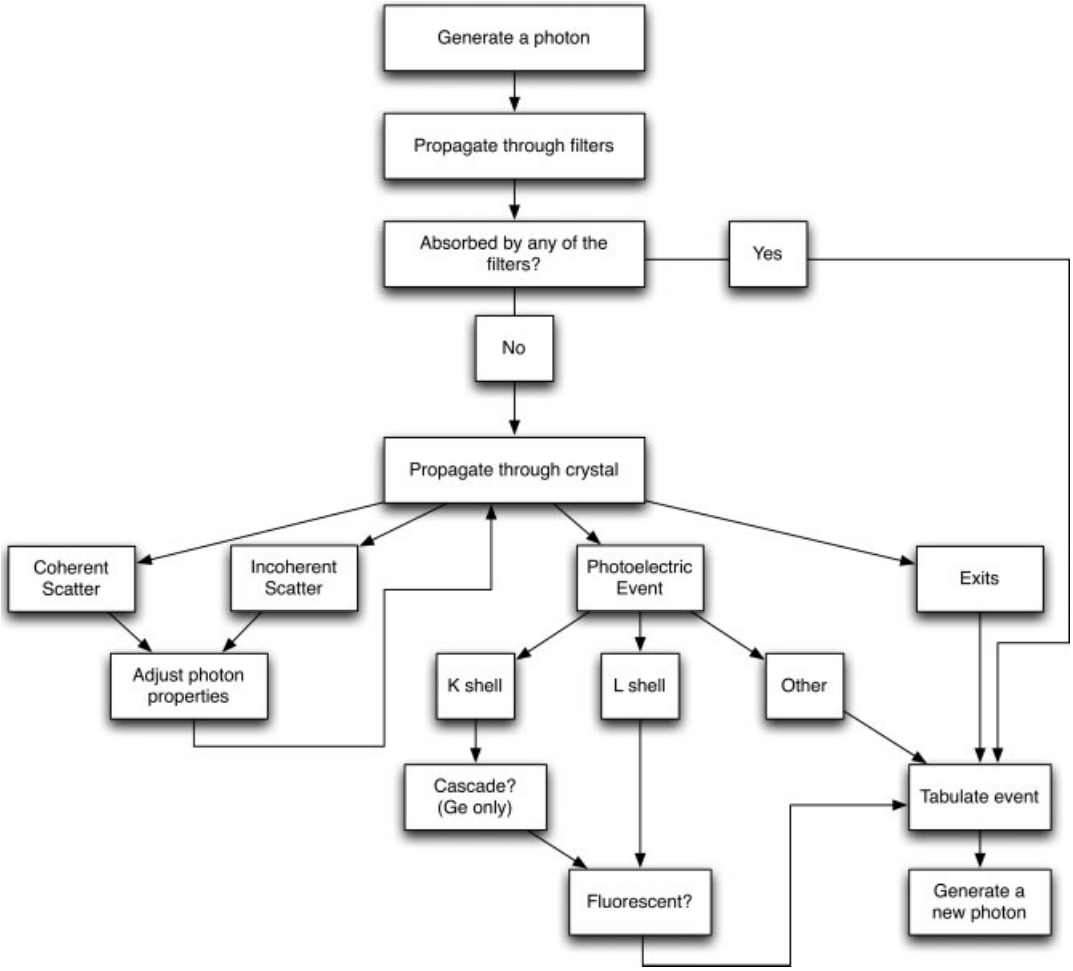

Figure 1. A flowchart of the program's calculation algorithm for a single photon. The program simulates a large number of photons, and then tabulates and outputs the results.

the length) of a filter to be zero, and the filter will have no effect on the photon. The only required dimension (other than those characterizing the source, the detector and the geometry between them) is the inner radius of the outer collimator, as this is used to calculate the solid angle(s) involved in the efficiency calculation. If no outer collimator is present, the aperture of the window should be used instead to provide a reasonable value for the program.

There are still limitations on the geometric parameters of the system, though. The detector crystal must be circular, as do the collimators (if either or both is present), and the source cannot be an arbitrary shape. While it is entirely possible, from a computational standpoint, to allow for non-circular crystals or collimators, or arbitrarily shaped sources, accounting for any or all of these possibilities would add considerable complication to the computation and would significantly increase the runtime of the program. Ensuring that the system is accurately described by the user would be more difficult, as having a crystal without axial symmetry requires knowledge of the orientation of the crystal relative to the source and the collimators, and this is both non-trivial and possibly not well known for encased detectors. While there are currently a few detectors that use non-circular crystals (e.g. the arrays discussed by Doyle[10] and presented here in more detail in Section *Handling Arrays of Detectors*), these are well approximated as circular crystals. This work can be considered, in light of this, as a first level of generalization in efficiency computation; in the future, higher levels of generalization can be considered, including non-circular crystals and arbitrarily shaped sources and collimators.

The Database

A simulation is only as accurate as the database it relies upon, and the database compiled here comes from several sources. The majority of the cross section data is taken from XCOM online.[11] The only cross section data not taken from XCOM is the photoelectric cross section data used when an atom in the detector crystal undergoes a fluorescent event. In this case, the cross sections of each atomic subshell are needed, rather than the data as a whole. The XCOM data is not split into subshells, so the data from Scofield[12] is used instead, and this data is somewhat problematic. The L edges in Scofield's data are located in slightly different places than the L edges given by Deslattes *et al*.,[13] so when this data is used in combination with the XCOM data (which uses the newer L edge values), there may be discrepancies. The low-resolution and tightly clumped values in the L edge region in the Scofield data compound the problem. We have performed some careful interpolation to adjust the Scofield data so that the L edges lie in the same place as they do in the XCOM data (and subsequently Deslattes' work), and while the numerical values are reasonable,

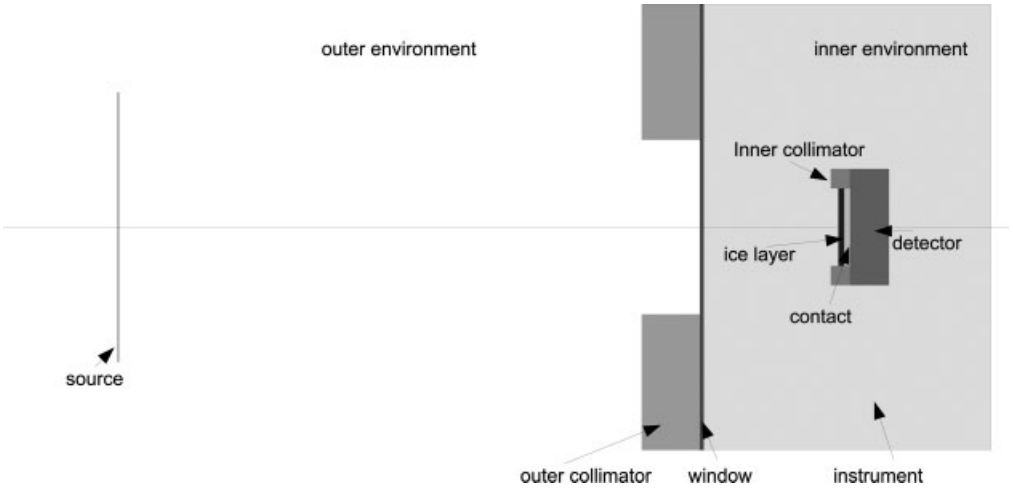

Figure 2. A schematic drawing of the general detector system. All quantities are variable, and individual components may not be present. Schematic is not to scale.

they should be considered only with a strong caveat. Fortunately, this affects only the structure of the L escape peaks in germanium, as the K data is consistent in both germanium and silicon; the L escape peak is not considered in silicon. This issue is also discussed in Section *Analysis of Some Typical Systems and Discussion*.

None of the other quantities used in this program have any associated issues, fortunately. The fluorescence yields are taken from three sources. For silicon, the K fluorescence yield ω_K is taken from Campbell *et al*.[14] They determine ω_K using two different databases of attenuation coefficients and get values of 0.050 and 0.052 $\pm$ 2%; we use the average, 0.051, in this program. For germanium, the K fluorescence yield is taken from Bambynek's 1984 work as referenced by Hubbell,[15] and has a value of 0.546. The L shell fluorescence yields are taken from Krause,[16] and all three subshells are taken to have a ω_L of 0.014. Lastly, the number of L shell vacancies created from a K shell interaction is taken from Bambynek *et al*.'s work.[17] The total number of L vacancies per K event is 1.265, and the number of vacancies in each subshell are 0.156, 0.461 and 0.648 for the L1, L2 and L3 subshells, respectively. All the filters that may or may not be present are characterized by using the parameterization scheme from Orlic *et al*.[18]

Finite Sources and Tilted Sources

Up to this point, efficiency calculations assumed that the source is a point source, and while this is a very good approximation when the distance between the source and the detector is large compared with the size of the source, this is not always the case. Sources are often extended, and in some situations, the source may be very close to the detector as in Ref. [10]. Treating the finite source as a single entity causes difficulties in defining the solid angle. To avoid this, finite sources are treated in this program as collections of point sources: the user defines the shape of the source (point, circular and square sources are all handled) and the program randomly determines a place on the source's surface, emits a photon from that location and proceeds as if the source were a point source. This is powerful because this approach deals with tilted sources just as easily; there is no restriction for the plane of the source to be parallel to the plane of the detector, and the finiteness of the source is ignored once the photon's point of emission is determined.

The Solid Angle

The solid angle is easily defined if the point of emission is a point rather than a finite shape, which is the principal reason that this approach was used. The term 'solid angle' is appropriate when one photon is being discussed, but any calculation of an average solid angle associated with a finite source should be carefully considered. The solid angle is not well defined if a finite shape is being considered, and this is what led us to the treatment of finite sources as collections of point sources. The solid angle needs to be calculated to make the program more efficient. If the photon can be generated with any directional angles, the vast majority of the photons will miss the system entirely, let alone the detector. Defining a small wedge of valid combinations of directional angles means that all of the photons hit the system, and most of them will make it through the outer collimator.

The back face of the outer collimator is used as the limiting aperture for this purpose, so the inner radius of the outer collimator is the important value. In systems where there is no outer collimator, a dummy value of this radius is used (and the collimator thickness is set to zero) which ensures that all the straight trajectories that will hit the detector are included in the wedge of validity. In general, the solid angle is defined as

$$\int d\Omega = \int_{(\cos\theta)_{\min}}^{(\cos\theta)_{\max}} \mathrm{d}(\cos\theta) \int_{\phi_{\min}}^{\phi_{\max}} \mathrm{d}\phi$$
$$= [(\cos\theta)_{\max} - (\cos\theta)_{\min}][\phi_{\max} - \phi_{\min}] \quad (4)$$

The maximum values of the propagation angles are easily determined using the positions of the elements of the system and will vary depending on where the photon originates. Because of this, the solid angle must be calculated for each simulated photon when the source is finite. An average solid angle for the source can be found, but using this to compute the efficiency gives very inaccurate results. Using the average solid angle calculated when the program is run properly (i.e. the solid angle is calculated for each individual point source considered on the extended source) for a source with radius 0.5 cm positioned 2 cm away from the detector face (and 1.5 cm to the outer collimator) gives efficiencies that are about 70% too low. This is an admittedly extreme example, but clearly the efficiency should be calculated one photon at a

time, using the solid angle properly calculated for each individual photon.

K and L X-Ray Escape Peaks

This program accounts for the K escape peak in silicon and both the K and L escape peaks for germanium. Because the cross section data below 1 keV is questionable, no photons with energy below 1 keV are handled. The energies of the silicon L transitions are no more than 150 eV, so the L escape peak is not handled. The L transitions for germanium range in energy from around 1.0 to 1.4 keV, so the L escape peak is handled. The K escape peak for both silicon and germanium detectors is handled rigorously. Up to six transitions comprising the K escape peak can be accounted for, and each line is treated independently. These transitions include the Kα, Kβ, as well as shake satellites and a radiative Auger contribution. The shake satellites are not accounted for for germanium detectors, but the Kα and Kβ lines are each split into their two components. The details of the silicon escape peaks and relative intensities are taken from Ref. [6]. All the transition energies used are those of Deslattes *et al*.[13]

A random number selects which line the fluorescent photon belongs to, and two other random numbers determine the propagation angles. The X-ray is treated like an incoming photon, and if it leaves the crystal, it contributes to the escape peak rather than the number of photons that scatter out of the detector. If it remains in the crystal, it is indistinguishable from an incoming photon, though its history is retained. The complete count of all fluorescent X-rays that leave the crystal at each incoming source energy is tabulated at the end of the program, as well as the breakdown by specific energy. A complete energy spectrum, with the main peak, all the escape peaks and the Compton features, is also provided in one of the output files. The escape peak intensity is presented as a percentage of the main peak intensity, and the escape peaks are summed over the component lines; the germanium L escape peak is not split by subshell. Energies that fall in the middle of the range of the germanium L lines, and thus between subshells, are treated properly. Each photon is assessed as to which processes are available to it, and nothing is assumed.

The L escape peak is more complicated not only because there are three subshells, each with a set of several lines, but also because there are two mechanisms available for L X-rays to be emitted from the detector crystal. L X-rays can be emitted, like K X-rays, through a direct process, where the incident photon interacts with the L shell and a fluorescent photon follows, but they can also be emitted through an indirect process after a K shell event. A K shell event may trigger a cascade effect, where L electrons drop to fill the vacancy left in the K shell, and a fluorescent L X-ray is emitted to conserve energy. This process is only available above the K edge, but when it is available it dominates over the direct process, as many more K shell interactions occur than L shell.

If the user prefers to apply his or her own escape peak model, the escape peak computation can be shut off. If only the K escape peak is needed, the L escape peak can be shut off for germanium detectors.

Efficiency Calculation Comparisons

Calculating the efficiency is straightforward, though the notion of calculating the efficiency of a single photon is somewhat counter-intuitive. Because all the photons are tracked explicitly, there is no need for any filter modelling or corrections for multiple interactions or escapes. All that is needed is a flag that is tripped when the photon is detected, another that is tripped if a fluorescent photon then leaves the detector, and the solid angle calculated for the individual photon. All the physics are accounted for in determining if and how the photon interacts in the first place, or if the fluorescent photon escapes. The expression is then just

$$\varepsilon_1 = \frac{(d-e)\Omega}{4\pi} \tag{5}$$

where d is the flag tripped when the photon is detected, e is the flag tripped when a fluorescent photon escapes and Ω is the solid angle. The total efficiency is a sum over the individual efficiencies scaled by the number of photons simulated:

$$\varepsilon = \frac{\sum_{\text{photons}} \varepsilon_1}{n} \tag{6}$$

For the simplest source–detector geometries, for example, a point source situated on the axis of a collimated detector, at a distance such that no photons encounter the curved edges of the crystal, our method should give results similar to the simple analytical model.[3,4] But the approximation in the latter whereby the crystal absorption term employs only the photoelectric cross section ensures that the results will not be identical. At lower energies this approximation overestimates the efficiency, whereas at higher energies the opposite is the case. For more complex geometries, especially those where short source–detector distances and finite area sources are encountered, edge effects are more likely, and further differences appear.

For the analytical model, we used the GUCSA subprogram provided within the GUPIX package,[9] in which multiple interactions, finite source areas and detector edge effects are all ignored. If results from GUCSA are adjusted for multiple interactions using the appropriate corrections detailed in O'Meara and Campbell,[5] they can be used as a basis for comparison with the results obtained by this new program. Because GUCSA provides only relative efficiencies ε_R (i.e. without an absolute solid angle factor), whereas the present program calculates absolute efficiencies ε, we chose first to compare ratios $\varepsilon_R(E_1)/\varepsilon_R(E_2)$ and $\varepsilon(E_1)/\varepsilon(E_2)$ where E_2 lies in the central energy region in which little variation in efficiency occurs, and E_1 is sampled throughout the energy range of the detector. The results agree within a percent for the majority of the tested energies, though the high- and low-energy results were differed slightly. GUCSA assumes that all the photons propagate parallel to the axis of symmetry of the detector crystal, whereas this new program makes no such assumption. The low-energy results are consistent with slightly more photons being absorbed by the filters, due to the slightly longer distance they travel through the filters, in the new program as compared with the old results. We used a collimated detector to eliminate any edge effects, but at high energies some photons may still escape. A comparison of our results with the GUCSA results is shown in Table 1. The results match within a percent for energies in the middle of the energy range, but below 5 keV and above 20 keV, the results diverge. This divergence highlights the limitations of the analytical model: as long as the system is 'nice' it works very well, but when the physical system starts to differ from the idealized system, the results differ significantly.

Table 1. A comparison of our results with the GUCSA results. The tabulated numbers are the ratio of $\varepsilon(E_1)/\varepsilon(E_2)$ to $\varepsilon_R(E_1)/\varepsilon_R(E_2)$, where ε is the efficiency we calculate via Monte Carlo, and ε_R is the relative efficiency calculated by GUCSA. To compare absolute and relative efficiencies, ratios are taken of the data within each data set, and then those ratios are compared to examine the differences between the two approaches. The GUCSA values have been corrected for multiple interactions to show that when those are accounted for and the geometries are close to ideal, the two approaches give very similar results. Note especially the consistency at high energies when $E_2 = 17.479$ and $E_2 = 22.162$

E_2(keV)	$E_1 = 9.887$	$E_1 = 17.479$	$E_1 = 22.162$
1.041	0.988	0.976	0.975
1.741	1.009	0.996	0.996
2.642	1.017	1.004	1.004
3.691	1.007	0.994	0.994
6.403	0.999	0.986	0.986
8.048	1.002	0.989	0.988
9.887	1.000	0.987	0.987
17.479	1.013	1.000	1.000
22.162	1.013	1.000	1.000
30.972	1.009	0.996	0.996
36.026	1.003	0.990	0.990
41.456	0.992	0.979	0.979
49.128	0.987	0.974	0.974

To illustrate this divergence, three situations are considered. Three considerations that cause the system to diverge from the idealized model are the inclusion of multiple interactions, the effect of using a finite (uncollimated) crystal and a finite source. These are all exacerbated if the source is close enough to the detector crystal for the distribution of photon trajectories to be closer to isotropic than to a parallel beam. To this end, we attempt to isolate each effect and compare it with the GUCSA results for an idealized system. To isolate the effect of neglecting multiple interactions, the detector is collimated and a point source is used. To isolate the edge effects, the detector is left uncollimated, and a point source is used. Finally, the effects of a non-ideal source are examined by using a collimated detector and a source with a non-zero radius. The effect of neglecting multiple interactions in the second two examples can be estimated by considering the results of the first comparison; shutting the multiple interactions off in the simulation defeats the purpose of rigorously calculating the detector's efficiency. The effect of an isotropic distribution of photon trajectories, rather than a parallel beam, can be estimated by considering the results of the comparison of the relative efficiencies in the so-called 'nice' geometry.

For this comparison, we use the absolute efficiencies rather than the relative efficiencies; the GUCSA results can be converted to absolute efficiencies by calculating a solid angle factor based on the geometry of the system (and assuming a point source). We simulated a typical Si(Li) detector at a variety of energies. The detector used was 4.3 mm thick, with a radius of 5.0 mm. It sat 5.0 mm behind an 8-mm thick Be window and had a Ni electrode. For the comparisons, the detector was simulated both with and without a 4.0 mm radius collimator on the face of the crystal, and the source was consistently placed 10.0 mm from the face of the detector crystal. Because GUCSA assumes that the incoming photons are all parallel to the axis of symmetry of the system, the close distance was chosen to enhance the discrepancy between the assumed trajectories of the photons in GUCSA and the physically realistic trajectories. The data is plotted in Figure 3; the top and bottom panels show the results from the collimated and uncollimated detector crystals, respectively.

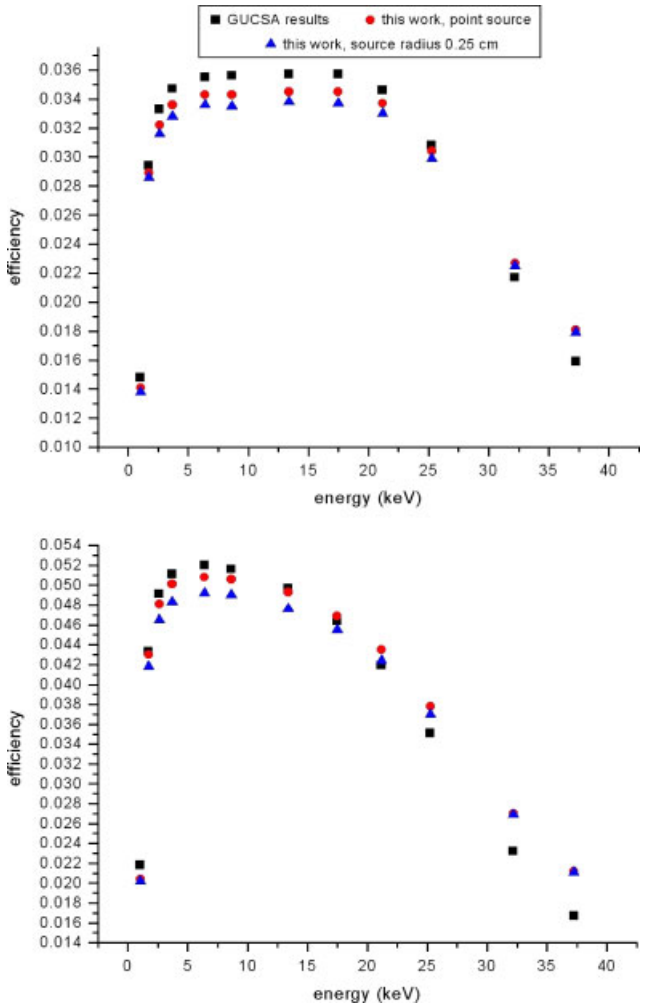

Figure 3. Comparison of absolute efficiencies from GUCSA and this work. Both panels have the sources 10 mm from the face of the detector crystal. The top panel shows the results for a Si(Li) detector of radius 0.5 cm with a 0.4 cm radius collimator, whereas the bottom panel shows the results for a 0.5 cm radius uncollimated Si(Li) detector. A point source and a finite source of radius 025 cm are compared. Note both the systematic changes between the data sets, and the difference in curves associated with an uncollimated detector crystal.

The red dots on the first panel show the data isolating the effect of neglecting multiple interactions. The detector is collimated, and the source is an ideal source, so at high energy, the discrepancy between this work and the GUCSA results is due to neglecting multiple interactions. At high energies, the effect discrepancy reaches about 15%. The blue triangles on the same plot show the effect of a finite source; at high energies, the effect of including multiple interactions is necessarily also present. The finite source data is consistently around 2% smaller than the point source data, except at the edge, where the data is very close. The effect of a finite source is mitigated to some degree by the high absorption in the filters (at low energies) and the escape of photons from the detector crystal at high energies. The particulars of variation in efficiency as a point source becomes finite are further explored in Section *Analysis of Some Typical Systems and Discussion*. Lastly,

edge effects are explored by using an uncollimated detector, and the data is shown in the bottom panel of Fig. 3. The red dots show the data from a point source, and the shape is similar to the curves obtained with a collimated detector. The flat middle region is smaller, as higher energy photons can more readily escape out the sides of the detector, and the discrepancy between the GUCSA results and this work is exacerbated. The blue triangle again show the data from a 0.25-cm radius source and are again between 2% and 3% lower than the point source data, except at the edges of the energy region for, presumably, similar reasons as the collimated detector. We are, of course, considering the edges only in terms of photon escape; no attempt has been made here to determine how many events are degraded by escape of Auger electrons and photoelectrons through the edges.

Analysis of Some Typical Systems and Discussion

The main feature of this new program is the range of geometries that it handles. It is expected that finite, off-axis and tilted geometries will all give different results than on-axis point sources. The effect of each of these three alterations can be tested easily by gradually increasing the radius of the source, or moving a point source further off-axis, or tilting a finite source while holding all the other geometric quantities fixed. This is best done over a range of energies, so as to accurately characterize the system. For analysis of the results from the program, a typical Si(Li) and a typical germanium detector were simulated. Both detectors had a radius of 5 mm and a 4-mm radius collimator attached. The Si(Li) detector was 4.37 mm thick, whereas the Ge detector was 10 mm thick. The source was consistently placed 2.0 cm from the detector face, with a 3.0 cm collimator to define the solid angle of each event. The detectors both had a Ni electrode and a 0.0125-mm thick Be window. The large collimator is used for consistency because the sources will be placed up to 2.0 cm from the detector's axis.

Efficiency calculations

To look at the effect of a non-ideal geometry on efficiency, three groups of simulations were run: one where a point source was moved progressively further from the axis of symmetry of the detector, one where a point source on the axis of symmetry became progressively more finite and a third where a finite, on-axis source was progressively tilted towards the detector face. In each group, a collection of typical energies was simulated, as low-energy photons will be affected differently by a changing geometry than high-energy photons. Figure 4 shows plots of efficiency for both silicon and germanium detectors over a range of energies typical for that detector. Note that the energies plotted are different for the two detector types but consistent for each detector.

As expected, the shapes of the efficiency curves are consistent across the energies simulated, though of course the shapes themselves differ between the three groups. The curves have a very similar shape between the two detectors, though the amount of curvature is slightly different. The germanium curves tend to be slightly more exaggerated than those of the silicon detector. Moving a point source off-axis has the most dramatic effect of the three, whereas tilting the source barely has an effect at all. The shape of the curve tends to be exaggerated for low-energy photons and flattened for higher energy photons. Low-energy photons are more sensitive to an increased filter length, so increasing the path length in either the beryllium window or the nickel electrode by a small amount will result in a noticeable change in the number of low-energy photons absorbed, and subsequently the efficiency.

Moving the source off the axis of symmetry causes a smooth decline in efficiency, with a drop of around 65% for both silicon and germanium as the source moves to 2 cm from the axis of symmetry. In silicon, the low-energy sources drop a few percent more than average, and the high energy drops a few percent less. In germanium, though, there is no energy-dependent pattern. The effect in silicon is small, though, and could be statistical in nature. Note that this geometry has the point source as far away from the axis of symmetry as it is from the plane of the detector face, and in practice the source geometry is unlikely to be this exaggerated. The effect of a growing source is not nearly as dramatic, though a smooth decrease in efficiency is visible as the source grows. The effect is not nearly as strong as placing a point source at the outer edge of the finite source, because in the finite source, photons are emitted from points close or on the axis as well as points closer to the edge of the source. The efficiency drops about 10% for silicon and 12% for germanium as the source increases to 1.0 cm in radius. Tilting a source increases the efficiency slightly, as the solid angles of the photons in the half of the source that is now closer to the detector increase more than the solid angles of the other half decrease by being slightly farther away. The effect is small for a source with a radius of 0.5 cm, with the efficiency growing by less than a percent for silicon and about 2% for germanium as the source tilts to 45° with respect to the place of the detector. This behaviour is uniform across the energies simulated, because it is a result of a changing distribution of solid angles, which is independent of source energy.

Escape peak calculations

While the primary purpose is to evaluate the efficiency of non-ideal detector systems, the program also calculates the escape peak intensities, relative to the intensity of the main energy peak. The results for on-axis point sources can be compared with previous work, for both silicon and germanium. For silicon, the work of Campbell *et al*.[14] using monochromatic X-rays from a synchrotron, is used for comparison. Our results, presented in Table 2, agree very closely to the experimental results, with no difference more than 2.75%, and most under 1.5%. The experimental results are accompanied by uncertainties of about 2%.

For germanium, both the K and the L peaks can be considered, though the treatment of the L peak has complicating factors as described in Section *The Database*. The K peak is straightforward, and the results of our program can be compared with the work

Table 2. Escape peak intensities relative to the main peak for Si(Li). The second column contains our results, and the third column contains the experimental results of Campbell *et al*.[14]

Energy(keV)	η_{MC}	η_{exp}
3.00	0.01260	0.01264
3.99	0.00862	0.00876
5.00	0.00575	0.00575
5.99	0.00391	0.00398
8.31	0.00188	0.00183

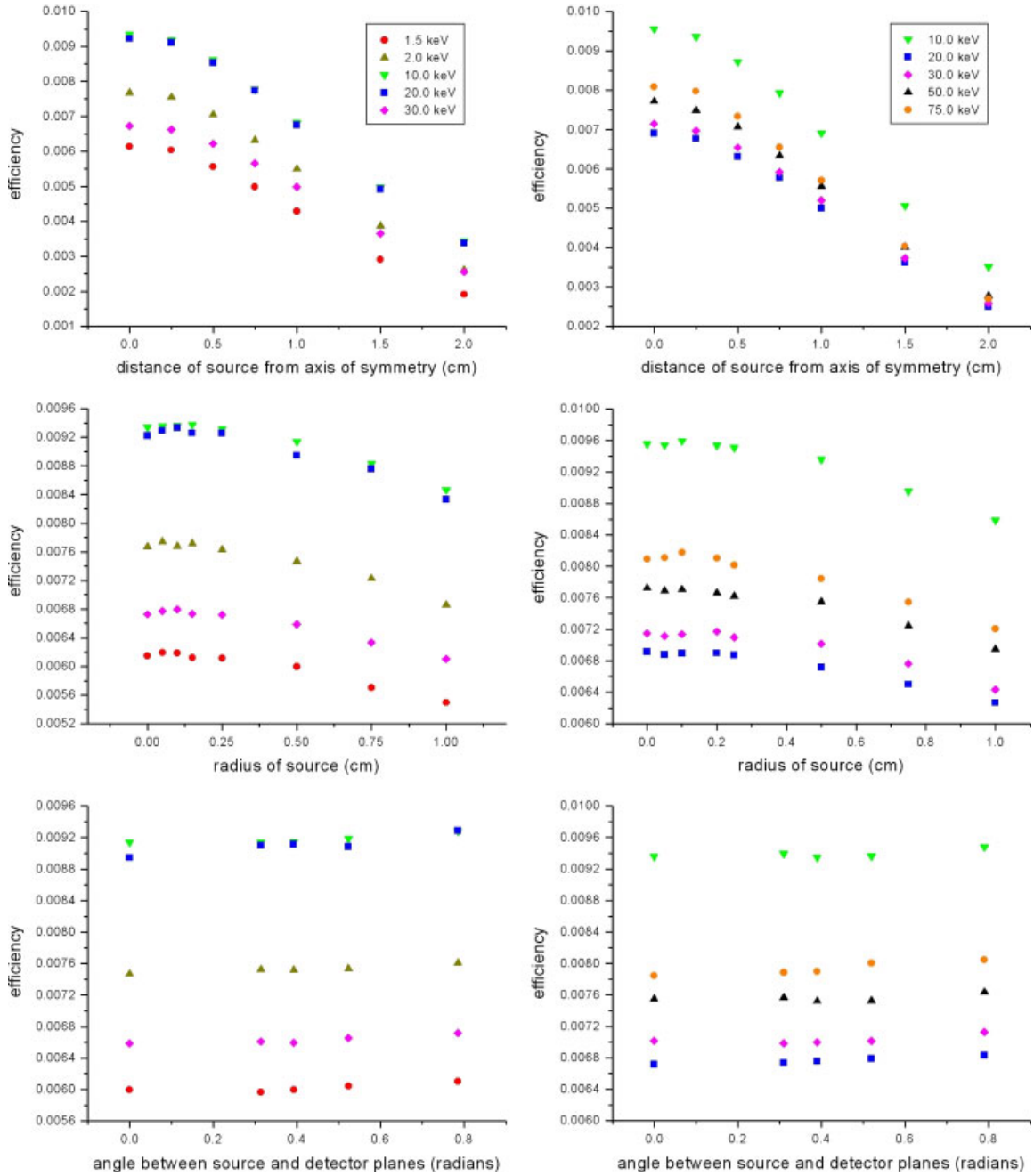

Figure 4. Three groups of simulations detailing how geometry affects the efficiency of the Si(Li) (left panels) and Ge (right panels) detectors discussed in the text. The top panels show a point source being moved off the axis of symmetry of the detector, the middle panels show a point source on the axis growing into a finite source and the bottom panels show a finite, on-axis source tilting towards the detector face. The symbols are consistent across all the panels for a given detector.

of Fioratti and Piermattei.[19] Fioratti and Piermattei devised an analytical formula to predict the relative intensity of the K escape peak in germanium detectors (and also NaI detectors, but these are not considered here) for three geometries. These geometries are labelled 'good', 'intermediate' and 'poor'; the 'good' geometry data is what is used here for comparison, as it corresponds most closely to the geometric setup we use. Our results are consistently about 20% higher than their results, but Fioratti and Piermattei account only for the K_α contributions to the escape peak; the K_β contributions are ignored, and these contributions are about 20% of those from the K_α lines. Because the discrepancy between the results matches with the expected contributions of the ignored K_β lines, our results are reasonable. At higher energies, the discrepancy between results becomes much larger. At these energies, the scattering cross sections are no longer small in comparison with the photoelectric cross sections. Fioratti and Piermattei ignore any scattering effects, and consider only the photoelectric cross sections, whereas our program considers both the scattering and the photoelectric cross sections. Table 3 contains our results for both the K and L escape peaks, as well as Fioratti and Piermattei's results for the K escape peak.

Table 3. Germanium K and L X-ray escape peak relative intensities for a variety of energies. Detector is the same germanium detector described in the text, and the source is placed 2 cm from the detector face. The first two columns are the results of our program, whereas the last column contains the K escape peak ratio for the so-called 'good' geometry detailed in Fioratti and Piermattei[19]

Energy (keV)	K peak	L peak	Fioratti K peak
1.25	0.0	0.00293	
1.50	0.0	0.00290	
2.00	0.0	0.00218	
4.00	0.0	0.00062	
6.00	0.0	0.00022	
8.00	0.0	0.00009	
10.00	0.0	0.00008	
15.00	0.134	0.00887	0.112
20.00	0.0868	0.00873	0.0749
30.00	0.0369	0.00861	0.0330
40.00	0.0181	0.00891	0.0159
50.00	0.0101	0.00897	0.00860
60.00	0.00589	0.00861	0.00509
80.00	0.00306	0.00912	0.00218
100.00	0.00550	0.00865	0.00112

The L escape peak is always much smaller than the K escape peak, as the L shell fluorescence yield is about 2.5% of the K shell fluorescence yield. It is interesting, though, to note the change in intensity of the L escape peak as the source energy crosses the K edge. This sudden jump occurs because the second (and dominant) mechanism of excitation is available only above the K edge. As discussed in Section *K and L X-Ray Escape Peaks*, a fluorescent L X-ray may be emitted directly, as happens below the K edge, or it may be emitted as a result of the atom settling after a K shell event. This indirect mechanism dominates over the direct mechanism, as it is vastly more probable that photon will interact with the K shell than that photon interacting with the L shell and producing a fluorescent X-ray.

However, strong caveats accompany the L escape peak results, although these are artefacts of the data sets available rather than an intrinsic issue with how the program is constructed. The photoelectric cross sections for the detector crystal need to be split by atomic subshell to investigate the behaviour of the L X-rays, or any low-energy ($<$1.5 keV) source. As discussed in Section *The Database*, the only data available that is split by subshell is the Scofield data,[12] and the L edges are in slightly different locations than those of Deslattes *et al*.[13] The two data sets are used to create an interpolated data set just in the region around the L edges, and while it is reasonable, it is by no means definitive. This needs to be done because if the L edges are in slightly different places, a fluorescent photon that is determined to be of a certain energy may lie in a different location relative to the L edges in the Scofield data (which determines which shells are available for a fluorescent photon to be emitted from, and the relative probability that one will be emitted) and the XCOM data (which determines how that photon will propagate through the detector crystal). Clearly, the program needs to be self-consistent, so it is important that all the subshell edges fall in the same locations, even if that means that the data requires a caveat.

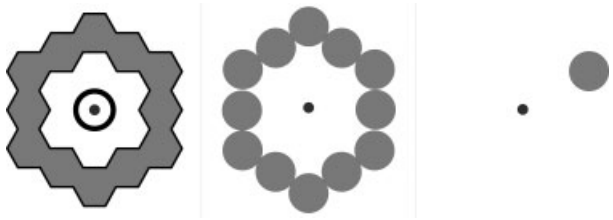

Figure 5. A schematic showing the detector array as shown in Ref. [10], how the detector array is considered for the purposes of this program and the situation that is actually simulated. In the first panel, the thick black outline around the hexagonal array is the tantalum ion collimator discussed in Ref. [10]. In all three panels, the black source can be either a point source or a finite, circular source.

Handling Arrays of Detectors

Recently, an annular SDD detector system has been built, with the benefit of increasing the solid angle subtended by the detector faces. The technical details are described by Doyle *et al*. in Ref. [10], along with an explanation of how these systems are valuable for μ-PIXE work. These arrays are potentially very useful, but the usual semi-empirical methods for calculating the detector efficiency are far from optimal, because the source sits off the axis of symmetry of the detector array. Because the source sits very close to the detector face (the detector sits about 3 mm behind the window, and the source sits either 1 or 6 mm in front of the window), it is inappropriate to assume a geometry where the source is on the axis of the detector face.

Only one detector is simulated, and the detector is taken to be the origin of the reference frame. In other words, the source is regarded as being displaced from the (single) detector, rather than the detector being displaced from the source (as is the natural way to discuss the complete, multi-detector system). This situation is handled natively by this program, and so no approximations or assumptions need to be made to calculate the efficiency. Once calculated for a single detector in the array, the efficiency is multiplied by the number of detectors in the array (here, 12). If the entire system was not symmetric, a more general approach would be needed, perhaps simulating each detector individually and then summing over the efficiencies. To date, all annular arrays of detectors are axially symmetric and are constructed in such a way that the detector + source system is also axially symmetric, so this is not yet an issue. Figure 5 shows first a schematic of the detector array as described in Ref. [10], then a schematic of how this geometry is interpreted for simulation, and lastly the situation that is fed into the program for simulating.

Using the quantities specified in Ref. [10], and assuming that there is no ambient or inner environment and a thin aluminium electrode, the efficiency is calculated at both operating positions. The source is assumed to be a point, because it is very finely focussed by a collimator at the centre of the array. The detectors are all the same, so the situation simulated is somewhat simplified. The detectors appear to be hexagonal, but our program only handles circular detectors. The same surface area is used, but this assumption introduces some error into the calculation. Moreover, Doyle's entire array is collimated, rather than each individual hexagonal detector (see the first panel in Fig. 5). Because some of the hexagons' sides touch, this means that some sides of an individual detector are collimated and some are not. It is unclear whether this collimator shadows the edge of detectors themselves or sits as a wall around their edges to protect stray particles from sneaking in the sides, and either way our program only handles

Table 4. Calculated efficiencies for annular detector arrays as described in Ref. [10]. A point source is positioned 4 and 9 mm from the detector face, as described in the paper

Energy (keV)	ε at 4 mm	ε at 9 mm
1.25	0.2208	0.0889
1.5	0.2817	0.1095
2	0.3371	0.1272
4	0.3880	0.1425
6	0.3924	0.1444
8	0.3895	0.1425
10	0.3640	0.1299
15	0.2184	0.0714
20	0.1139	0.0361
30	0.0362	0.0112

collimation all around a detector or not at all, so this collimator is not accounted for. The results for Doyle's entire array, for the same range of energies as shown previously, are shown in Table 4.

Conclusions

The program described here increases the user's capability to accurately quantify the efficiency of their detector system and handles geometries that are not easily handled by analytical methods. It also, however, highlights the need for improvements in the current cross section database. This program is only as accurate as the data it uses to describe the detector crystal, and there are significant issues around the L edges of germanium due to database uncertainties. The L escape peaks are nevertheless calculated and output, but should be considered with care until better subshell cross section data is available for use. The K escape peaks do not suffer from this problem and are described in detail. This program is especially helpful for describing new systems of annular detectors, which are difficult to quantify using previous analytical models. Because these are likely to become popular, as they are small, yet have a large detector surface area and thus a high efficiency, it is important that this program handle these detector systems. Finally, it is important to reiterate that the program does not as yet include any consideration of hot electron transport or charge carrier losses, and that it ignores the contribution to overall detection efficiency of the supporting pulse processor, whether analogue or digital. This latter issue is discussed by Papp *et al.*[8]

Acknowledgements

This work was supported by the Natural Science and Engineering Research Council of Canada. We would like to thank Bernie Nickel for invaluable help regarding the solid angle issue.

Appendix

This is an example of the detailed results output file for a point source located 1.0 cm from the detector crystal face for an energy of 30 keV. The files also list the number of events that undergo one or more incoherent interactions before a photoelectric event or undergo some combination of incoherent and coherent scatter events before a photoelectric event. For this simulation, there were no incoherent events, so these results were all zero.

Detailed results for system example:	
Input quantities	
all measurements in cm, radians, and g/cm^3	
Source and activity	
- Source radius:	0.00000
- Shape of source:	point
- Location of centre of source:	0.000, 0.000
- Photons generated:	5 000 000
Detector	
- Detector material:	Si
- Detector radius:	0.50000
- Detector thickness:	0.43000
System geometry	
- Source to detector distance:	1.00000
- Source to window distance:	0.49920
- Angle between source and detector	0.00000
Outer collimator	
- Inner radius:	2.00000
- Outer radius:	3.00000
- Thickness:	0.00000
Inner collimator	
- Inner radius:	0.40000
- Outer radius:	0.50000
- Thickness:	0.00000
Other geometry	
- Window thickness:	0.00080000
- Electrode thickness:	0.00000100
- Ice layer thickness:	0.00000000
- Dead layer thickness:	0.00000000
Materials and densities:	
- Window: 4(1)	1.8480
- Electrode: 28(1)	8.9020
Source energy: 30.000 keV	
Salient information	
- Efficiency:	0.0253
- Relative K escape peak intensity:	0.0202
- Relative L escape peak intensity:	0.0000
- Average depth of final interaction:	0.1609
- Effective solid angle:	2.0236
- Efficiency through outer collimator:	0.9252
Events	
- Photoelectric events (PE):	316 439
- PE with no scatter events:	301 231
- PE with scatter events:	5208
- Photons scatter out of detector:	13 259
- Photons pass through detector:	107 477
- Photons lost in detector (<1 keV):	0
Geometry	
- Photons that miss the system:	104 913
- Photons hit the outer collimator:	268 910
- Photons hit the collimator edge:	0
- Photons that miss the detector:	3 978 541
- Photons hit the detector:	645 305
- Photons hit the inner collimator:	208 094
- Photons hit active detector face:	437 211
- Photons escaping laterally:	54 860
- Photons escaping out front:	736
- Photons escaping out back:	65 140

Escape peak	
- Photons that fluoresce:	14 854
- Fluorescent events that escape:	6261
- K shell fluorescent escapes:	6261
Filters	
- Outer environment:	0
- Outer collimator:	0
- Window:	2331
- Inner environment:	0
- Inner collimator:	208 094
- Electrode:	36
- Ice:	0
- Dead layer:	0
Multiple events	
- Coherent + Photoelectric:	
1	14 545
2	634
3	27
4	2
5	0
6+	0

The code's output has recently been augmented to include intrinsic efficiencies. This term describes the fraction of those photons originally traveling towards the detector dace that result in a full-energy event. An effective solid angle can be derived from the ratio of the intrinsic and absolute efficiencies.

References

[1] N. V. de Castro, R. J. A. Levesque, *Nucl. Instrum. Methods* **1967**, *46*, 325.
[2] K. M. Wainio, G. F. Knoll, *Nucl. Instrum. Methods* **1966**, *44*, 213.
[3] J. S. Hansen, J. C. McGeorge, D. Nix, W. D. Schmidt-Ott, I. Unus, R. W. Fink, *Nucl. Instrum. Methods* **1973**, *106*, 365.
[4] D. D. Cohen, *Nucl. Instrum. Methods* **1980**, *178*, 481.
[5] J. M. O'Meara, J. L. Campbell, *X-ray Spectrom.* **2004**, *33*, 146.
[6] J. L. Campbell, G. Cauchon, M.-C. Lepy, L. MacDonald, P. Plagnard, P. Stemmler, W. J. Teesdale, G. C. White, *Nucl. Instrum. Methods Phys. Res., Sect. A* **1998**, *418*, 394.
[7] F. Scholze, M. Procop, *X-ray Spectrom.* **2009**, *38*, 312.
[8] T. Papp, A. T. Papp, J. A. Maxwell, *Anal. Sci.* **2005**, *21*(7), 737.
[9] J. A. Maxwell, W. J. Teesdale, J. L. Campbell, *Nucl. Instrum. Methods Phys. Res., Sect. B* **1995**, *95*, 407.
[10] B. L. Doyle, D. S. Walsh, P. G. Kotula, P. Rossi, T. Schulein, M. Rohde, *X-ray Spectrom.* **2005**, *34*, 279.
[11] M. J. Berger, J. H. Hubbell, Xcom: Photon Cross Sections on a Personal Computer, Technical Report NBSIR 87–3597, National Bureau of Standards, Office of Standard Reference Data: Gaithersburg, MD 20899, **1987**.
[12] J. H. Scofield, Theoretical Photoionizations Cross Sections from 1 to 1500 Kev, Technical Report UCRL- 51326, Lawrence Livermore National Laboratory Report, **1973**.
[13] R. D. Deslattes, J. E. G. Kessler, P. Indelicato, L. de Billy, E. Lindroth, J. Anton, *Rev. Mod. Phys.* **2003**, *75*, 35.
[14] J. L. Campbell, G. Cauchon, T. Lakatos, M.-C. Lepy, L. McDonald, T. Papp, J. Plagnard, P. Stemmler, W. J. Teesdale, *J. Phys. B: At. Mol. Opt. Phys.* **1998**, *31*, 4765.
[15] J. H. Hubbell, P. N. Trehan, N. Singh, B. Chand, D. Mehta, M. L. Garg, R. R. Garg, S. Singh, S. Puri, *J. Phys. Chem. Ref. Data* **1994**, *23*(2), 339.
[16] M. O. Krause, *J. Phys. Chem. Ref. Data* **1979**, *8*(2), 307.
[17] W. Bambynek, B. Crasemann, R. W. Fink, H.-U. Freund, H. Mark, C. D. Swift, R. E. Price, P. V. Rao, *Rev. Mod. Phys.* **1972**, *44*(4), 716.
[18] I. Orlic, K. K. Loh, C. H. Sow, S. M. Tang, P. Thong, *Nucl. Instrum. Methods Phys. Res., Sect. B* **1993**, *74*, 352.
[19] M. P. Fioratti, S. R. Piermattei, *Nucl. Instrum. Methods* **1971**, *96*, 605.

